Heliyon 6 (2020) e04597

Contents lists available at ScienceDirect

Heliyon

journal homepage: www.cell.com/heliyon

Research article

A modelling study to evaluate the effect of impure CO_2 on reservoir performance in a sandstone saline aquifer

Mohammed Dahiru Aminu [a,*], Vasilije Manovic [b]

[a] Department of Geology, Modibbo Adama University of Technology, Yola, Nigeria
[b] Centre for Climate and Environmental Protection, Cranfield University, Bedford, Bedfordshire, MK43 0AL, UK

ARTICLE INFO

Keywords:
Chemical engineering
Petroleum engineering
Energy sustainability
Geomechanics
Geotechnical engineering
Basin analysis
Reservoir engineering
Carbon capture and storage
Saline aquifer
Impurities in CO_2
Reservoir performance
Storage capacity
Modelling and simulation

ABSTRACT

Carbon capture and storage (CCS) is expected to play a key role in meeting greenhouse gas emissions reduction targets. In the UK Southern North Sea, the Bunter Sandstone formation (BSF) has been identified as a potential reservoir which can store very large amounts of CO_2. The formation has fairly good porosity and permeability and is sealed with both effective caprock and base rock, making CO_2 storage feasible at industrial scale. However, when CO_2 is captured, it typically contains impurities, which may shift the boundaries of the CO_2 phase diagram, implying that higher costs will be needed for storage operations. In this study, we modelled the effect of CO_2 and impurities (NO_2, SO_2, H_2S) on the reservoir performance of the BSF. The injection of CO_2 at constant rate and pressure using a single horizontal well injection strategy was simulated for up to 30 years, as well as an additional 30 years of monitoring. The results suggest that impurities in the CO_2 stream affect injectivity differently, but the effects are usually encountered during early stages of injection into the BSF and may not necessarily affect cumulative injection over an extended period. It was also found that porosity of the storage site is the most important factor controlling the limits on injection. The simulations also suggest that CO_2 remains secured within the reservoir for 30 years after injection is completed, indicating that no post-injection leakage is anticipated.

1. Introduction

The global emissions of carbon dioxide into the atmosphere, caused mainly by the burning of fossil fuels such as those from industrial processes (e.g., cement, steel and lime production), power and transportation sectors, have caused global warming and climate change [1]. Carbon capture and storage (CCS) has been considered as one of the viable climate change mitigation technologies, and it is expected to help in reducing over 20% of the global greenhouse gas (GHG) emissions by 2050, while its exclusion can cause over 70% increase in the global cost of meeting emission reduction targets [2].

The main options for CO_2 storage in underground geological formations are saline aquifers, depleted oil and gas reservoirs, unmineable coal seams, basalt formations, hydrate storage of CO_2 within the subsurface environment, and CO_2-based enhanced geothermal systems [3]. Among these options, storage in saline aquifers is considered as one of the most feasible choices for technology deployment, since they provide the largest potential storage volume [4] and are unsuitable for other uses.

Depending on the source of the captured CO_2, some impurities (usually $<5\%_{vol.}$ [5, 6]) are contained in the CO_2 stream. The type and amount of impurities in the CO_2 stream may have a significant effect on the physical qualities of the storage reservoir. The presence of impurities can alter the molar volumes and shift the boundaries in the CO_2 phase diagram to higher pressures, which implies higher operating pressures and cost may be required for CO_2 storage [3]. Therefore, the overall storage capacity can be adversely affected [7]. On the other hand, the possible short term effects of impurities on the reservoir performance may indicate the necessity of a change in injection strategy [7]. While it is crucial to quantify the long-term effects of impurities on storage sites in real life applications, it is equally important to note that laboratory experimental approaches are complex, costly and inadequately slow. Instead, numerical simulations can be used to accelerate the evaluation of impurity effects. Several numerical studies have been conducted to evaluate the long-term reservoir performance when impure CO_2 is injected into geological formations [7, 8, 9, 10], and such studies suggest that the presence of impurities may cause a considerable influence on injection and storage mainly due to chemical reactivity of the host rock with formation water resulting in changes in permeability and porosity. For example, the presence of SO_2 could lead to the formation of strong acids, which could then cause further dissolution and precipitation of

* Corresponding author.
E-mail address: mdaminu@mautech.edu.ng (M.D. Aminu).

https://doi.org/10.1016/j.heliyon.2020.e04597
Received 6 May 2020; Received in revised form 30 June 2020; Accepted 27 July 2020

rock minerals. Additionally, the presence of impurities in the injected CO_2 and the subsequent geochemical reactions with saline water and minerals in the host rock can lead to the precipitation of authigenic or secondary mineral phases which could effectively lock up the stored CO_2 in immobile secondary phases for geologic timescales [11].

Waldmann et al. [7] studied the physicochemical effects of discrete CO_2–SO_2 mixtures on injection and storage in order to assess the impact on overall storage capacity in the Ketzin injection site, Germany. In their study, they considered geological conditions in the Ketzin site, and they assessed the impact of SO_2 on the physicochemical behaviour of the CO_2 phase by geochemical modelling of fluid-rock interactions. Since variations in porosity and permeability of the host rock can negatively influence CO_2 storage capacity, the results obtained from chemical models on porosity and permeability were integrated into the reservoir simulations to assess likely impacts. Results from their study revealed that the presence of SO_2 caused a significant reduction in porosity compared to pure CO_2 during the period of injection. Their results also suggested that the overall impact of SO_2 ($<1\%_{vol.}$) was low, although the morphology changes due to chemical reactions reduced the pore spaces available for storage. Similarly, Wang et al. [9] studied the impact of SO_2 on CO_2 injectivity in the Basal Cambrian sandstone saline aquifer in Western Canada. In their study, $2.5\%_{vol.}$ SO_2 was used, and they reported, for the first time, that enhanced quartz dissolution due to the effect of SO_2 apparently caused significant precipitation of NaCl, which could reduce the permeability of reservoir rocks.

To the best of our knowledge, numerical models capable of evaluating long-term reservoir conditions during injection and storage of CO_2 and impurities have not been previously utilised [3], given that the current research is mainly focused on the thermophysical properties of impurities that are inevitably present in the CO_2 stream. However, it is worth noting that these properties can be confidently predicted from knowledge of the temperature, pressure and brine chemistry [12]. To further de-risk CO_2 storage, it is important that research is conducted in understanding the effect of impurities introduced through the CO_2 stream on the thermophysical properties of the CO_2-brine system of the reservoir [12]. Therefore, in this study, we evaluate the effect of CO_2 and impurities (NO_2, SO_2 and H_2S) during injection and storage in a sandstone saline aquifer. We evaluate their effects on key reservoir performance indicators, i.e., well bottom-hole pressure, CO_2 injection rate, field pressure and cumulative gas injection using a single horizontal well injection strategy for a 30-year period, and an additional 30-year period of monitoring. The Bunter Sandstone formation (BSF) in the southern sector of the UK North Sea was selected as a case study. A simplified model for reservoir simulation to evaluate the reservoir performance during injection and storage using time and specific observation point indices was developed.

2. Numerical model

2.1. Reservoir model and boundary conditions

To develop the model of the BSF for flow simulations, we used simplified box models where the geology and domain of research were characterised as horizontal layers and representative bulk values were assigned for the various reservoir properties using data from laboratory experimental analysis [13] and the open literature. The injection and storage of CO_2 into the BSF saline aquifer was simulated using the ECLIPSE E300 compositional simulator which can model fluid flow as a multiphase and multicomponent system. A similar reservoir simulator (ECLIPSE E100 black oil) was used in previous studies [14, 15, 16, 17, 18] on CO_2 storage, without considering the composition of injected fluids and the effects of impurities on reservoir performance. For a compositional simulation involving a multicomponent run, the key parameters that account for each impurity case are the experimentally determined permeability values, volume of each component in the injection stream and diffusion coefficients of components in water.

The simulation process involves several steps (Figure 1) which include inputting data to the CO2STORE module of the simulator that conform with reservoir properties of the targeted storage formation; the use of lithostatic pressure gradient for model validation with respect to the injection depth; and conducting sensitivity tests with respect to grid dimensions in order to select the grid that provides optimum injection within the targeted reservoir. The rock and fluid properties used for multiphase flow simulations are presented in Table 1. A grid of $10 \times 10 \times 3$ cells (300 grid cells in total) was used, and the model dimension was discretised into 90 km $\times$ 90 km $\times$ 3 km. Notwithstanding that the grid is coarse, an adaptive mesh refinement for optimising the reservoir performance was not conducted in the simulation as it is known that for a single injector that seeks to store CO_2 over a storage region of large lateral extent such as the BSF, even a less refined mesh provides an accurate representation of the reservoir performance [19, 20, 21].

The depth to the crest of the Bunter storage structure was 1171 m [22], and the thickness of the BSF at the storage point was 215 m [22]. Therefore, we used 1171 m as depth of the top face of the grid block, and we adopted 1181 m as injection depth. To validate the model against lithostatic pressure gradient, 0.165 bar/m was used. This was chosen as a typical value for lithostatic pressure gradient reported by Energy Technologies Institute (ETI) [22] for the Bunter storage development plan and is close to values used by Noy et. al. [23] and Williams et al. [17]. Additionally, in order not to suffer mechanical failures at any point during injection operations, the simulation was initially run (with the average porosity and average permeability values of the BSF derived by ETI [22]) and injection pressure was limited to 90% of the lithostatic pressure (175 bar) at injection depth (1181 m). The pressure constraints from our simulations were found to be in good agreement with anticipated pressure, and we established that our model runs within safe injection pressure. Moreover, the injection operations are expected to be free from any sanding risks due to geomechanical issues. The analysis of existing wells within the BSF suggest that the reservoir is relatively strong and sand failure events around the near wellbore area [22], which could cause subsequent operational problems, are unlikely.

Saline aquifers are usually very large as they cover hundreds of km^2 and the BSF is not an exception (Figure 2). Therefore, modelling for CO_2 storage in saline aquifers is usually focused on the area affected by the CO_2 plume distribution [17], which is usually around the injection point and surrounding regions. However, in selecting an appropriate reservoir size for modelling, it is important to note that a fairly considerable aquifer size should be adopted since pressure footprint due to injection can extend much further in the aquifer [17, 23, 24] to cause unrealistic pressure build-up in the model [17]. Therefore, in this study, the optimum reservoir size was obtained by conducting simulations with various grid sizes and correlating the results with available pressure data [22]. The grid dimension was kept constant while the grid block size was varied in the DX and DY directions by a deduction of 20 m from the previous grid block size in each subsequent simulation. The variation of these grid blocks was then limited to reservoir sizes that were capable of sustaining CO_2 injection for the specified 30-year period. In order to select the optimum reservoir size, we used a method proposed by ETI [22] for the Bunter storage development plan, which suggests that optimum reservoir size could be selected from a grid in which the injection rate can be maximally sustained.

It is generally agreed that the boundaries of a reservoir can influence the pressure build-up and storage capacity. The most conventional estimate is the assumption that all horizontal and vertical boundaries of the model are closed [19, 24]. However, for CO_2 storage applications over injection timescales and subsequent migrations of <100 years, the boundary conditions are found to have a negligible impact on reservoir performance [25]. This is due to the large areal extent of the Bunter region [25]. Therefore, we believe that our results are valid for both sets of open and closed boundary conditions since they are based on reservoir performance evaluation over this timescale [25].

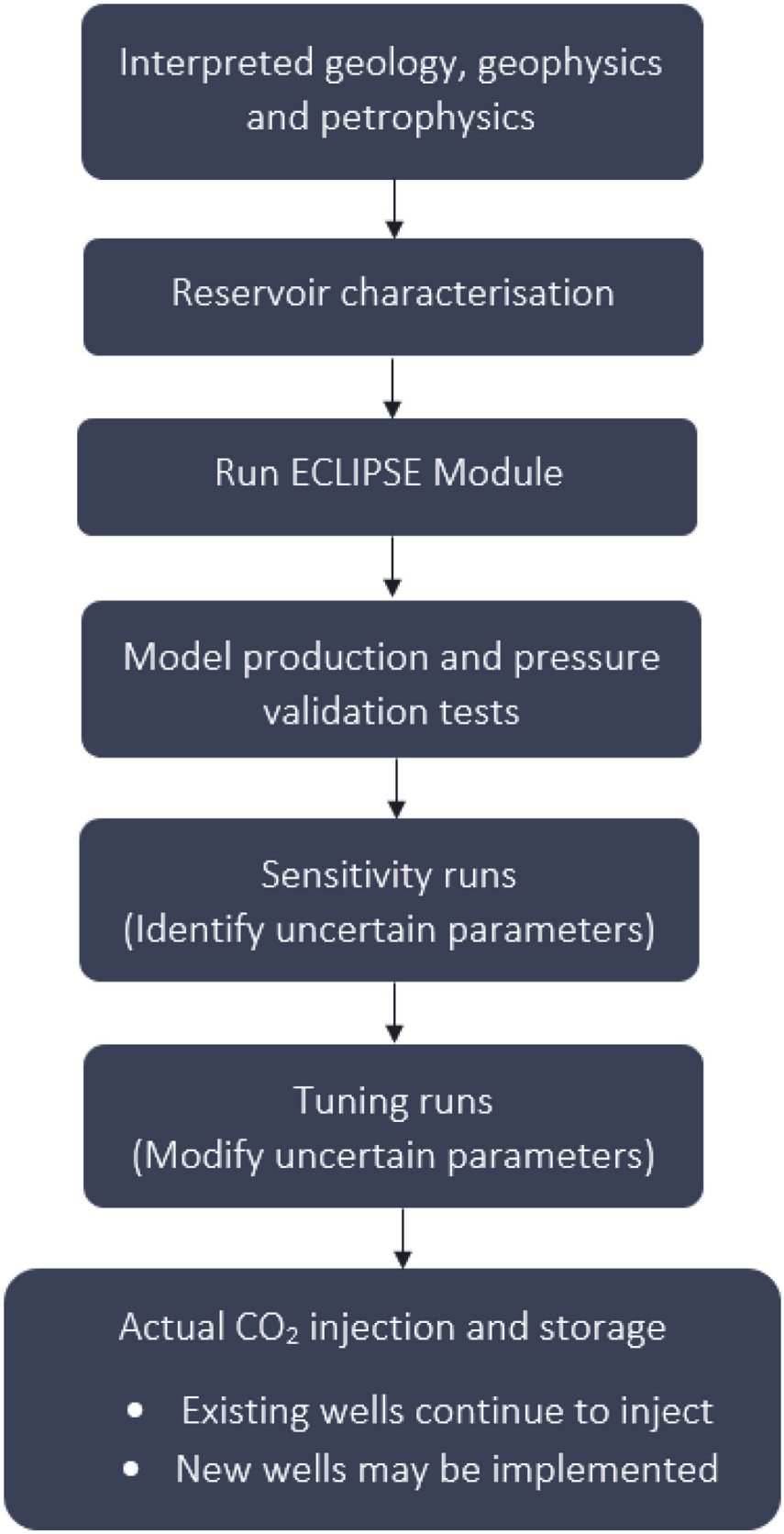

Figure 1. The workflow for numerical simulation.

Table 1. Rock and fluid properties used for the simulations.

Parameter	Value	Unit	Reference
Grid dimension	10 × 10 × 3	-	-
Grid block size	300 × 300 × 10	m	-
Porosity (lower and upper limits for all model runs)	10, 22	%	Vincent [26]
Permeability (variable depending on impurity present)	254 [a], 140 [b], 225 [c], 255 [d]	mD	Aminu et al. [13]
Depth to top face of grid block	1171	m	ETI [22]
Reference depth	1181	m	-
Model datum depth	1181	m	-
Initial reservoir temperature	37	°C	ETI [22]
Average reservoir pressure	124	bar	ETI [22]
Bottom-hole pressure limit	175	bar	
Content of impurity in the CO_2 stream	5	$\%_{vol}$	[5, 6]
Diffusion coefficients of components in water	3.0×10^{-4} (H_2O [e]), 1.4×10^{-4} (CO_2), 1.0×10^{-4} (NaCl [f]), 1.21 (NO_2 [g]), 0.0001 (SO_2 [h]), 0.0002 (H_2S [i])	m^2/day	[e]Mills [27]; [e]Holz et al. [28]; [f]Guggenheim [29]; [g]Dekker et al. [30]; [h]Koliadima et al. [31]; [i]Haimour and Sandall [32].
Diffusion coefficients of components	0.232 (H_2O), 1.382 (CO_2)	m^2/day	Cussler [33]
Rock density	2300	kg/m^3	ETI [22]
Lithostatic pressure gradient	0.165	bar/m	ETI [22]
Pore compressibility	4.5×10^{-10}	Pa^{-1}	Zhou et al. [34]; Noy et al. [23]
Fluid injection rate	6×10^6	Sm^3CO_2/day	-
Injection period	30	Year	-
Monitoring period	30	Year	-

Note: a, b, c, and d, denote permeability values obtained after exposure to CO_2, CO_2–NO_2, CO_2–SO_2 and CO_2–H_2S, respectively.

2.2. Reservoir and fluid properties

The BSF was deposited during the late Permian and Triassic periods (Figure 3). It comprises pebbly sandstones and sandstones intercalated with small amounts of conglomerates, mudstones and siltstones. The reservoir formation is typically 200 m thick and has fair to good porosity and permeability, and occurs at depths of about 1000–3000 m [23]. The BSF is also overlain primarily by the Triassic mudstones of the Haisborough Group which act as caprock or seal and it is underlain by the Permian Bunter Shale and the evaporitic strata of the Zechstein Group [35, 36, 37].

At the grid block scale of the reservoir, two different porosities, 10 and 22%, were considered for simulations, which agree well with the lowermost and uppermost intervals of the BSF in the southern sector of the UK North Sea based on selected borehole neutron logs [26]. The permeability values were experimentally determined by Aminu et al. [13] using empirical relationships to account for variations in reservoir grain size distributions from rock samples exposed to CO_2 and impurities for a period of 9 months using simulated reservoir conditions. The permeability in the vertical direction was derived from a generic vertical-to-horizontal permeability ratio of 1:10 and this agrees well with the work of Heinemann et al. [39]. We assume that the overlying and underlying boundaries of the model are impermeable due to the presence of effective caprock and base rock. Therefore, we do not anticipate any fluid flow out of the simplified reservoir model compartment.

There are very limited relative permeability data for CO_2-brine systems from North Sea formations [17, 22]. Therefore, uncertainties might exist in understanding the relative permeability of the reservoir. Nevertheless, we used data from ETI [22] for the Bunter storage development plan, which were derived by endpoint inputs from available experimental values. The reservoir was assumed to have an initial temperature of 37 °C and initial average pressure of 124 bar.

With reference to CO_2 and impurities, the main properties of the simulated fluids considered as inputs in the model runs were the percentages of both CO_2 and an associated impurity within the injection stream, and the diffusion coefficients of all components in water and air, which were experimentally determined by different workers as presented in Table 1. The fluid properties of the injection stream (e.g. viscosity) and properties of the formation water (e.g. pH) are not required inputs in a compositional model run as these are determined by the simulator in each run. The acceptable level of impurities in the CO_2 stream are determined based on a combination of environmental, safety and economic considerations [3]. Typically, the CO_2 stream is expected to have a purity level of around 90%$_{vol.}$ [40]. The National Energy Technology Laboratory (NETL) [41] and the Dynamis project [42] have recommended the limits of impurities for CO_2 stream components as a benchmark for CO_2 capture, utilisation and storage (CCUS) systems [43]. In any transport and storage applications, the concentration of air-derived non-condensable species, e.g. N_2, O_2, Ar, is recommended to not exceed 4%$_{vol.}$ [43] while other species may not exceed 5%$_{vol.}$ [5, 6] due to effects on compression and storage systems [43]. Consequently, the impurity levels adopted for this study agree well with recommendations in the literature for guidelines on conceptual studies.

2.3. Governing equations

For the multiphase flow model used in this study, the governing equations for simulation of CO_2 injection for storage into a saline aquifer are like those used for oil, water, and CO_2 flows through porous reservoirs. Darcy's law, which incorporates mass and energy conservation equations, as reviewed by Jiang [44], was used for the simulations.

$$q = -\frac{k}{\mu}(\nabla p - \rho g) \tag{1}$$

Using Eq. (1), it is possible to calculate velocity through the porous medium:

$$v = \frac{q}{\varnothing} = -\frac{k}{\mu\varnothing}(\nabla p - \rho g) \tag{2}$$

In terms of the positive z-direction as vertically up (opposite to gravity), multiphase extension of Darcy's law can be used for an individual fluid phase α, thus:

$$v_\alpha = \frac{q_\alpha}{\varnothing} = -\frac{kk_\alpha}{\mu_\alpha\varnothing}(\nabla p_\alpha - \rho_\alpha g\nabla z) \tag{3}$$

For CO_2 storage, the flow is modelled as a multiphase which requires considering CO_2, brine, rock, and multicomponents such as the CO_2 and water system. Thus, the number of components and phases can differ depending on application. In Eq. (4), the conservation of mass is expressed by the balance of four components that represent all possible mechanisms of mass transfer, which are: temporal rate of change of mass at fixed point, which can also be referred to as the local derivative or fixed term; convective mass transport; diffusive mass transport; and sink or source term for mass.

$$\frac{\partial}{\partial t}\left[\varnothing\sum_{\alpha}\left(\rho_{\alpha}s_{\alpha}X_{i}^{\alpha}\right)\right]+\sum_{\alpha}\nabla\left(\rho_{\alpha}X_{i}^{\alpha}q_{\alpha}\right)-\sum_{\alpha}\nabla\left(\varnothing s_{\alpha}\tau_{\alpha}D_{\alpha}\rho_{\alpha}\nabla X_{i}^{\alpha}\right)=Si \tag{4}$$

The gas phase diffusion coefficient for each component is also accounted for in a compositional run. These are used to define diffusive flows in terms of vapour mole fractions. The normal diffusion coefficients are defined by the following condition (Reid et al. [45]):

$$J_i=\ -cD_i\frac{\partial y_i}{\partial d} \tag{5}$$

These diffusion coefficients are used in the compositional model run to obtain gas inter-block diffusive flows, which take the form:

$$F_{ig}^{diff}=\ T_D D_{ig}\left(S_g b_g^m\right)\Delta y_i \tag{6}$$

For CO_2 storage reservoir simulations, the capillary forces are significant both in residual and structural/stratigraphic trapping. In the seal or caprock, the threshold of the capillary force can be high enough to keep the non-wetting phase, which can be CO_2 fluid or gas phase, from entering small pore throats in the seal. The capillary force also keeps bubbles of the CO_2 phase in an immobile state in small pore spaces of the reservoir during CO_2 migration. Thus, capillary pressure, which is the pressure difference between the non-wetting phase and wetting phase in a porous medium, is given as:

$$P_c=P_n-P_w \tag{7}$$

The compositional model run uses a modified Peng-Robinson equation of state [46] which is able to correctly compute the density, viscosity and compressibility of CO_2 as a function of temperature and pressure, as well as the mutual solubility of CO_2 and brine.

For the density of brine and CO_2, the determination of amount of CO_2 that will be dissolved in brine is important for the estimation of storage capacity and in understanding the interactions between CO_2-brine-rock because of low pH or acidity of CO_2-saturated brine [47]. Since the dissolution of CO_2 in brine influences the solution density, the influence of dissolved CO_2 on brine is expressed thus:

$$\rho=\rho_b+M_{CO_2}C-C\rho_b V_{\phi} \tag{8}$$

2.4. Model study design

In this study, we designed a reservoir simulation case to evaluate the limits of stability of various chemical phases in the CO_2 stream with respect to operational uncertainties. This allowed us to account for the likely uncertainties that could arise in the deployment of CO_2 storage in the BSF with different impurities in the injection stream using surface flow rate as the well control mode. In practice, a CO_2 injection project could operate with multiple injection wells, e.g., the In Salah project [48, 49, 50], or single injection well, e.g., the Sleipner project [1]. However, the number of injection wells that can be deployed for any storage project may vary depending on several factors such as the reservoir heterogeneity [19], the amount of CO_2 which can be injected into a single well without causing adverse overpressure [51], the trade-off between cost of

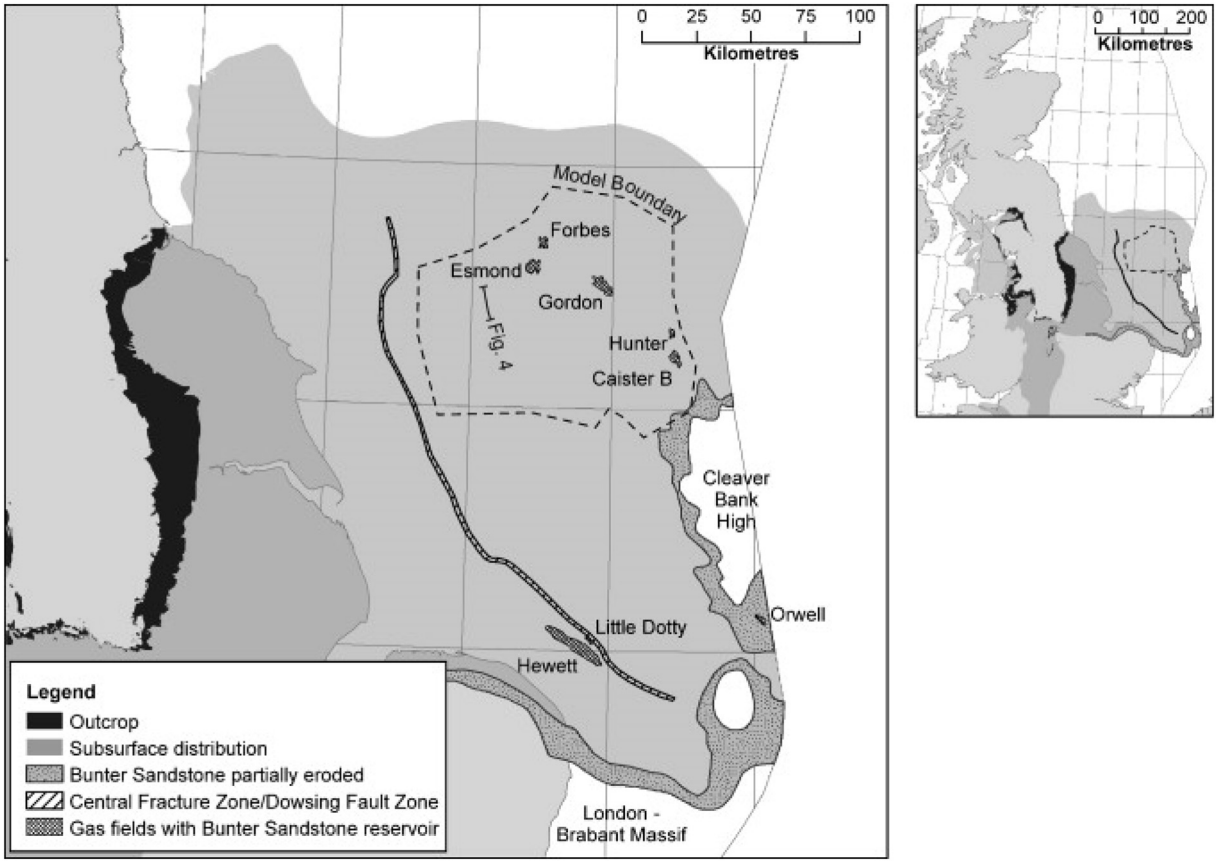

Figure 2. Distribution of the Bunter Sandstone formation in the UK sector of the southern North Sea [23].

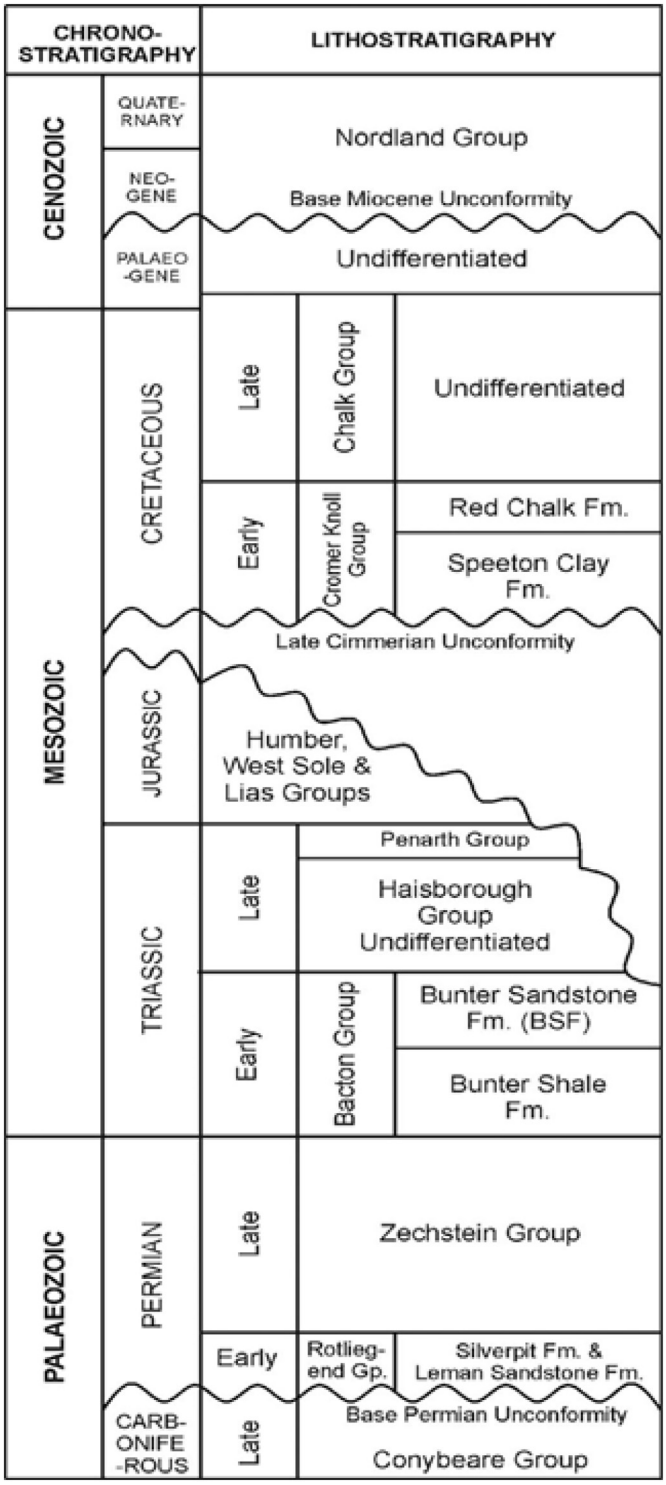

Figure 3. A generalised stratigraphy of the UK sector of the southern North Sea [38].

adding a well [19] and/or the amount of CO_2 that could be taken by any single well.

Previous studies on CO_2 storage in the BSF [17, 19, 23, 39] suggest that the motivation for using multiple injection wells for storage is largely driven by the amount of CO_2 that could be taken by each well per year. Typically, industry practice has suggested that volumes ranging from 1-2 $MtCO_2$/year [19, 52] could be stored in geologic formations beneath the North Sea, and this can be achieved with 20 injection wells [19], or even 12 injection wells [19, 23]. Moreover, ETI [22] deployed 4 injection wells to store approximately 7 $MtCO_2$/year over a period of 40 years. A constant injection rate as well as a constant injection pressure for the entire period of injection were assumed. In practice, the CO_2 injection rate could vary to maximise injectivity. However, it must be noted that the limits of stability in the CO_2 phase diagram regarding the operational uncertainties occur during the well pressure build-up prior to stability. Thus, the variation of injection rate after peak pressure is attained could only lead to a reoccurrence of the shifts in the boundaries of the CO_2 phase diagram as it was in the case of the preceding injection rate. We also assumed that 6×10^6 Sm^3CO_2/day was made available from an industrial site and transported for injection at the storage site. Thus, 6×10^6 Sm^3/CO_2/day was set as injection rate, but the volume of CO_2 injected was initially dependent on the well control modes, although the injection will normally be affected by the pressure build-up in the reservoir. Since the allowable bottom-hole pressure for injection was set to 90% lithostatic pressure at depth, the constant injection pressure used during the storage period ensured that the limit was not exceeded.

While our modelling did not consider the likely effect of impurity on any change in reservoir porosity, so that initial porosity values from experimental data can be assigned in each impurity case as we did for changes in reservoir permeability obtained from laboratory experimental analysis [13], it does not imply that impurities could not have affected the porosity of the BSF, and hence its reservoir performance. However, our assumption for adopting the upper and lower limits of the BSF porosity as reported by Vincent [26] in these simulations was informed by the analysis of mineral phases of rock samples after exposure to CO_2 and impurities, as reported in our previous study [13]. From the results, we can infer that there could be a significant reduction in porosity due to dissolution of clay minerals such as mica [53, 54] and an increase in porosity due to the dissolution of quartz [55], feldspar and albite [56].

3. Results and discussion

After injection, CO_2 plume is expected to migrate to the top of a reservoir due to buoyancy and it gradually spreads out laterally. The force of buoyancy causes the less dense gas to rise over denser saline water. The pattern of plume migration occurs both laterally and vertically and is expected to behave in this way due to the absence of any geological barriers to flow. The presence of impermeable seals atop and beneath the storage formation is expected to keep the plume spreading across the radial distance of the reservoir. Figures 4 and 5 are sketches of flow processes during CO_2 injection and storage in the reservoir.

From a geochemical perspective, CO_2 and impurities can influence the storage system in basically three ways: formation of carbonic acid or bicarbonates by dissolution of CO_2 in formation water (Equations (9) and (10)); production of weak or strong acids due to the effects of impurities; and dissolution and/or precipitation of calcite as cementing material [13, 58, 59].

$$CO_2 + H_2O \leftrightarrow H_2CO_3 \quad (9)$$

$$CO_2 + H_2O \leftrightarrow H^+ + HCO_3^- \quad (10)$$

Unlike the dissolution of CO_2 in formation water, the introduction of NO_2 in the injection stream can produce a weak acid HNO_2 or a strong acid HNO_3, as given below (Equations (11) and (12)):

$$2NO_2 + H_2O \leftrightarrow HNO_2 + HNO_3 \quad (11)$$

$$3NO_2 + H_2O \leftrightarrow 2HNO_3 + NO \quad (12)$$

Similarly, the introduction of SO_2 in the injection stream can produce weak acids H_2SO_3 and H_2S and/or a strong acid H_2SO_4 in the formation water, as given thus (Equations (13), (14) and (15)):

$$SO_2 + H_2O \leftrightarrow H_2SO_3 \quad (13)$$

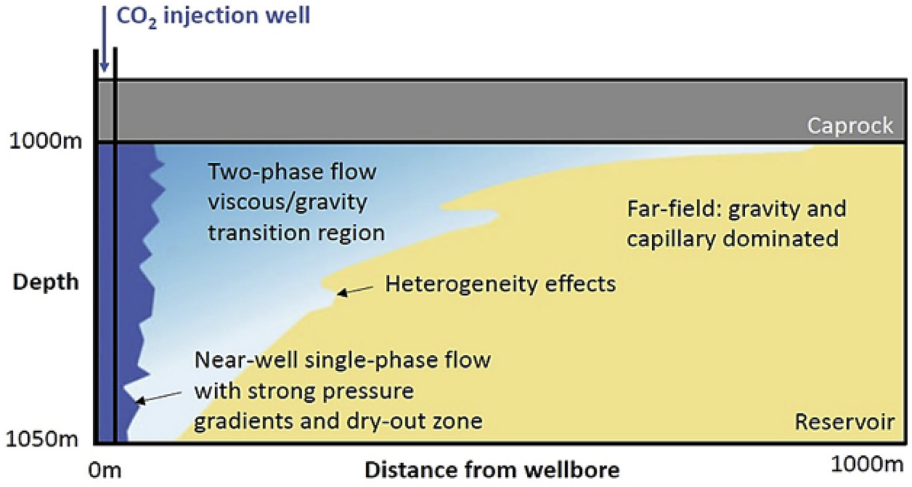

Figure 4. Sketch of flow processes and flow regimes for CO_2 injection into an ideal storage unit [57].

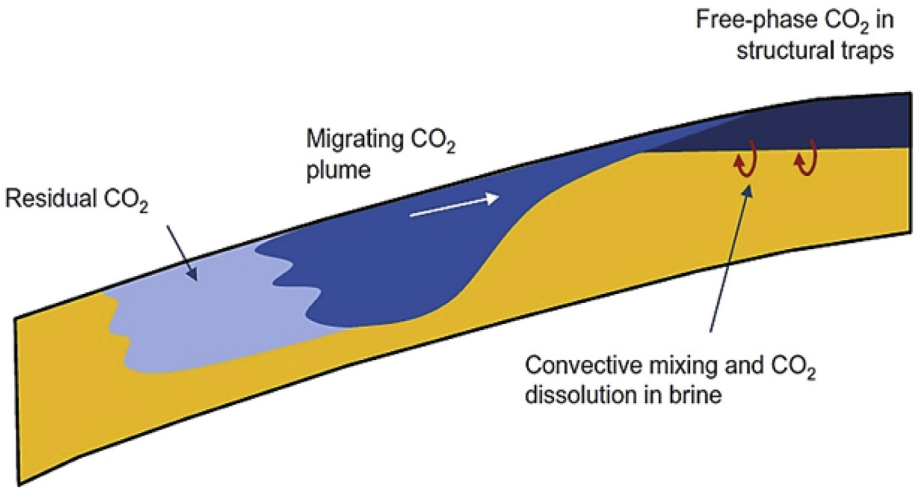

Figure 5. Sketch illustrating CO_2 storage flow processes [57].

$$SO_2 + H_2O \leftrightarrow \frac{3}{4}H_2SO_4 + \frac{1}{4}H_2S \quad (14)$$

$$SO_2 + H_2O + \frac{1}{2}O_2 \leftrightarrow H_2SO_4 \quad (15)$$

The introduction of H_2S in the injection stream can be explained thus (Equations (16) and (17)):

$$H_2S + H_2O \rightarrow HS^- + H_3O^+ \quad (16)$$

$$HS^- + H_2O \rightarrow S^- + H_3O^+ \quad (17)$$

In addition, the dissolution and/or precipitation of calcite involves a cascade of simultaneous reactions [60, 61, 62, 63, 64], as given thus (Equations (18), (19) and (20)):

$$CaCO_3 + H^+ \leftrightarrow Ca^{2+} + HCO_3^- \quad (18)$$

$$CaCO_3 + H_2CO_3 \leftrightarrow Ca^{2+} + 2HCO_3^- \quad (19)$$

$$CaCO_3 + H_2O \leftrightarrow Ca^{2+} + HCO_3^- + OH^- \quad (20)$$

In this study, the well bottom-hole pressure (WBHP) build-up in the reservoir was monitored at two periods which correspond to the first day of injection and the time it took to reach the peak pressure, for each simulation case, respectively. These observations enabled the determination of any potential effect of impurities on pressure perturbations and stability during injection. The WBHP build-up for storage sites with 10% and 22% initial porosity for pure and impure CO_2 storage is shown in Figure 6. For all storage sites, we observed a continuous increase in pressure until a maximum of 175 bar was reached, which then remained constant throughout the period of injection. However, for different simulation cases, the time to reach the maximum WBHP varied.

The WBHP of pure CO_2 injection into the storage site with 10% initial porosity reached its maximum pressure after 45 days of injection. In comparison to injection with impurities, the injection of CO_2–NO_2 resulted in the maximum pressure being attained within a relatively shorter period. Likewise, after the injection of CO_2–SO_2 and CO_2–H_2S, the time it took to attain maximum pressure in each case was the same as it was in the case of CO_2–NO_2.

For pure CO_2 injection into the storage site with 22% initial porosity, the WBHP reached its peak after 90 days of injection. In comparison to injection with impurities, the introduction of CO_2–NO_2, CO_2–SO_2 and CO_2–H_2S in each case, showed that maximum pressure was attained relatively faster than in the pure CO_2 case. The WBHP rise suggested consistency with reservoir porosity. Thus, for storage sites with lower porosity, the maximum pressure was attained relatively faster than for sites with higher porosity.

The corresponding well gas injection rate (WGIR) at three observation points is shown in Figure 7. The observation points were considered against the WBHP. These points correspond to the first day of injection

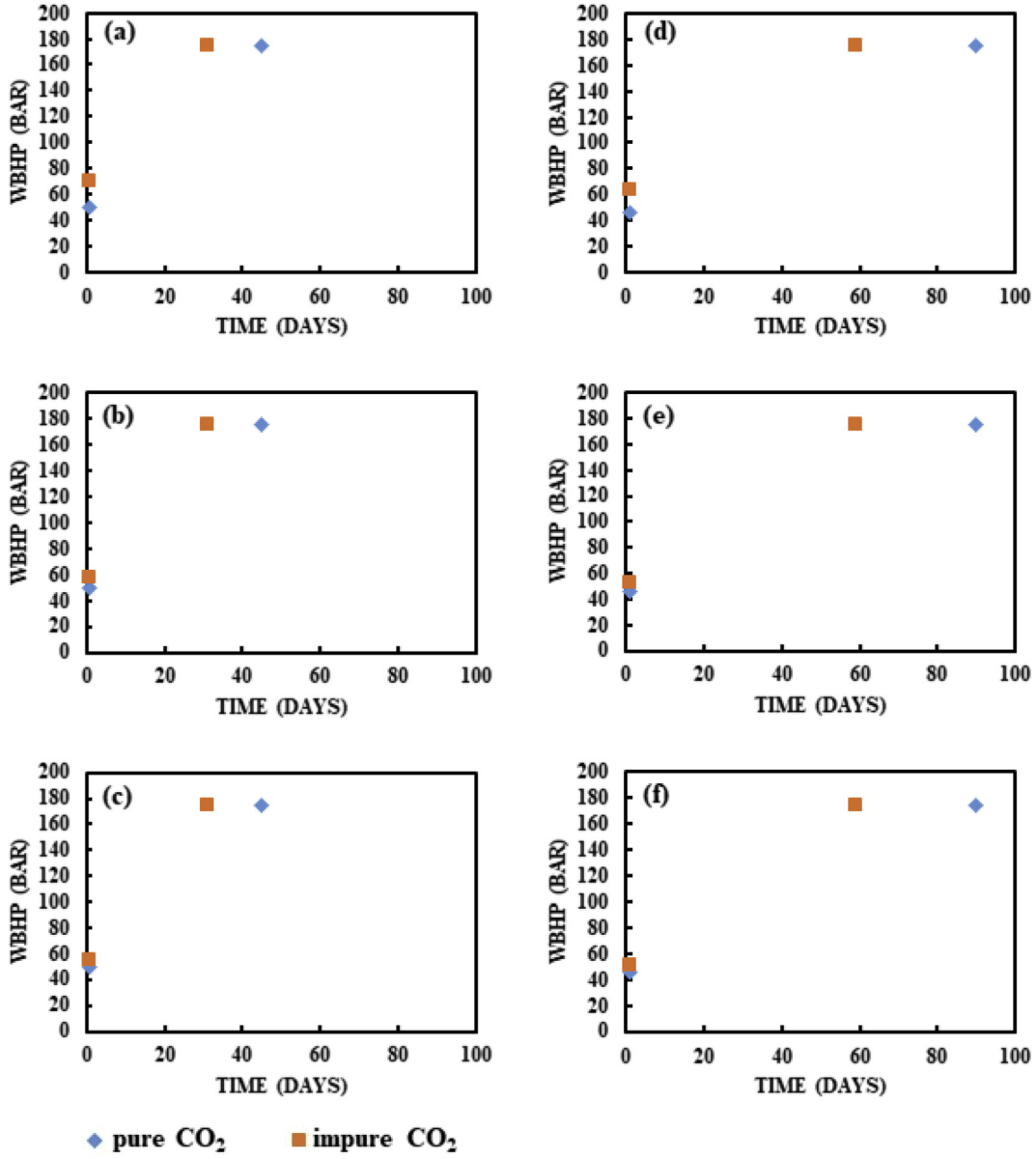

Figure 6. Well bottom-hole pressure (WBHP) build-up for pure and impure CO_2 storage for sites with 10% initial porosity ((a) CO_2–NO_2, (b) CO_2–SO_2, (c) CO_2–H_2S), and 22% initial porosity ((d) CO_2–NO_2, (e) CO_2–SO_2, (f) CO_2–H_2S).

(observation point index 1), the peak WBHP (observation point index 2) and the last day of injection (observation point 3). For all storage sites, we observed an initial injection rate of 6×10^6 Sm^3CO_2/day at observation point 1 and this rate remained constant until the WBHP attained stability when injection rate began to decrease with time until the well was shut.

The injection rate of pure CO_2 at the storage site with 10% initial porosity was 1.87×10^6 Sm^3 at observation point 2 (45 days). Since we did not consider a new injection rate at any time after the peak WBHP was attained, for all storage sites, we do not expect to have a significant volume of CO_2 to be injected when the well shuts. Therefore, the introduction of impurity, in each case, caused a significantly higher injection rate to be attained. For all the impurity cases, the injection volumes at this observation point were similar.

On the other hand, when pure CO_2 was injected in the storage site with 22% initial porosity, an injection rate of 3.1×10^6 Sm^3 was encountered at observation point 2 (90 days). The injection of CO_2–NO_2 caused a considerably higher injection rate to be encountered at the same observation point (59 days). Furthermore, the introduction of CO_2–SO_2 and CO_2–H_2S impurities, in each case, respectively, resulted in a considerably higher injection rate in comparison with the pure CO_2 case. It should be noted that these large degrees of difference in the injection rates at observation point 2, for all storage sites, may not necessarily be a strong factor that could cause a considerably lower injection volume in the long term.

The results from WGIR seem to show a correlation with the initial reservoir porosity and permeability, although the effect of porosity appears to be more overwhelming. We observed that a more porous injection site led to higher injectivity. However, this scenario was specific to observation point 2, for all cases.

Figure 8 shows the field pressure (FPR) at three observation points for sites with 10% and 22% initial porosity. The FPR was observed with respect to WBHP on the first day of injection (observation point index 1), peak WBHP (observation point index 2), and at the end of injection period (observation point index 3). For all cases simulated, we observed an increasing field pressure from an initial pressure of approximately 124 bar, and this increases gradually, without stabilising at observation point 2 until a peak pressure of 274 bar was attained. The peak FPR attainment

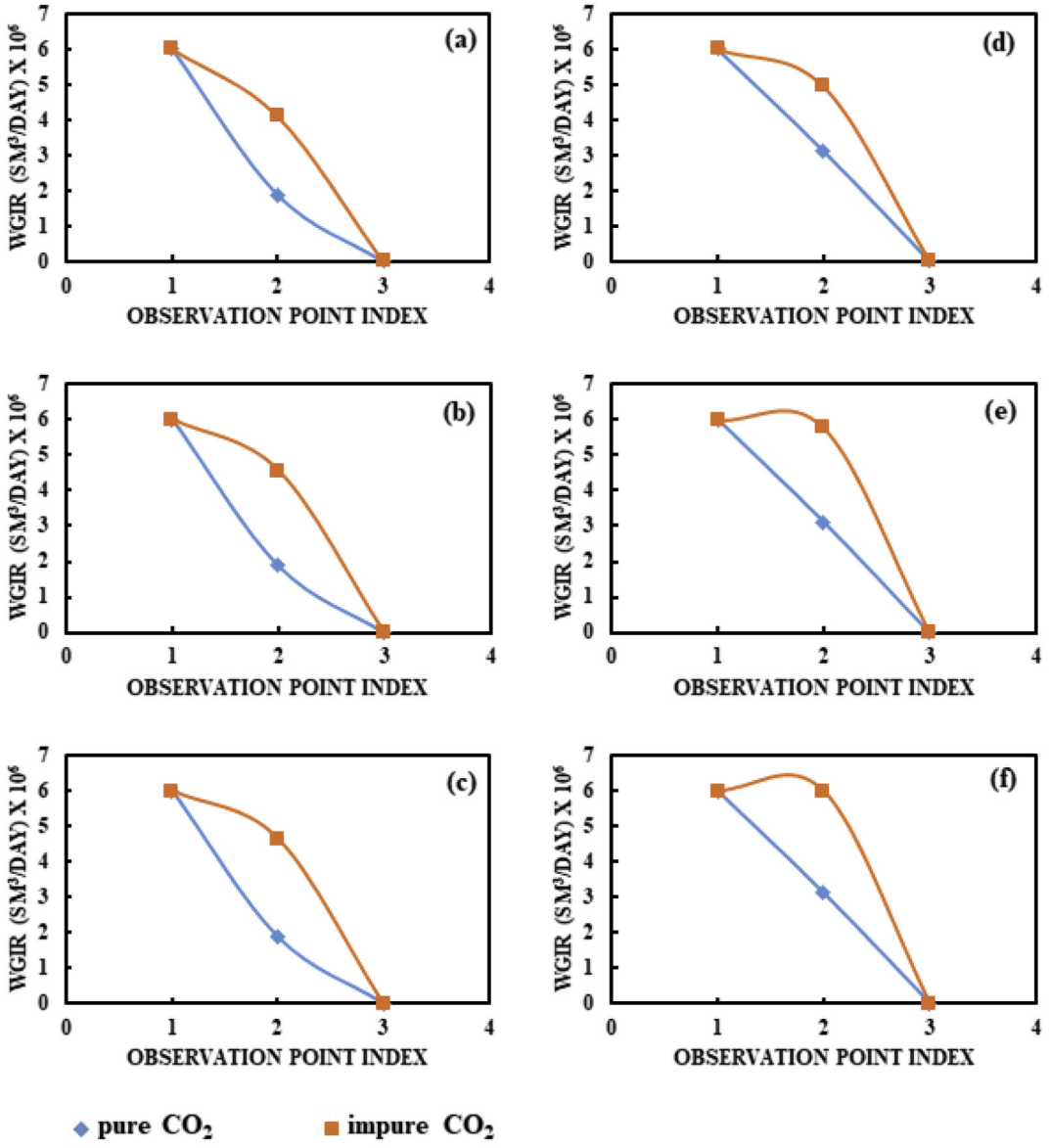

Figure 7. Well gas injection rate (WGIR) for pure and impure CO_2 storage for sites with 10% initial porosity ((a) CO_2–NO_2, (b) CO_2–SO_2, (c) CO_2–H_2S), and 22% initial porosity ((d) CO_2–NO_2, (e) CO_2–SO_2, (f) CO_2–H_2S).

time varies for each simulation case, and such pressure is always reached before the end of injection when the well is shut. The variation in FPR for various storage sites was a result of differences in the change in hydrostatic pressure which is affected by the bulk properties of the reservoir.

The FPR for pure CO_2 injection at the storage site with 10% initial porosity was 263 bar at observation point 2 (45 days) and 273 bar at observation point 3. When CO_2–NO_2 was injected, there was a reasonable decrease in FPR at observation point 2 (31 days) and nearly the same pressure was maintained as in the pure CO_2 case at observation point 3. The injection of both CO_2–SO_2 and CO_2–H_2S also led to considerable decreases in the FPR in comparison with the pure CO_2 case at observation points 2, respectively. However, as it is expected, for all impurity cases, there has not been as significant differences in the FPR as in the pure CO_2 case, for all impurity cases, respectively. Additionally, there was no significant discrepancy in FPR at the time the well was shut and at the end of the monitoring period. This suggests that the field pressure in the reservoir remained the same throughout the monitoring period, implying that reservoir containment is dependable.

In the storage site with 22% initial porosity, the FPRs encountered for pure CO_2 were 259 bar and 273 bar, at observation points 2 and 3, respectively. The injection of CO_2–NO_2 caused the FPR to decrease somewhat reasonably at observation point 2 (59 days), while there was an almost similar FPR at observation point 3, as with the case for pure CO_2 injection. Additionally, the injection of CO_2–SO_2 caused a considerable decrease in FPR at observation point 2 (59 days), while similar FPR was encountered in observation point 3, relative to the pure CO_2 injection case. Lastly, the injection of CO_2–H_2S also showed a significant decrease in FPR at observation point 2 (59 days), relative to the pure CO_2 case.

The well gas injection total (WGIT) for sites with 10% and 22% initial porosity is presented in Figure 9. This is also the same as the cumulative injection. The observation points were considered against the WBHP on the first day of injection (observation point index 1), the peak WBHP (observation point 2) and at the end of injection period (observation point 3). For all cases simulated, we observed an increasing CO_2 injection until the well was shut. Besides the effect of impure CO_2, which was manifest at observation point 2, the initial porosity of the storage site significantly controlled the cumulative injection.

Based on the findings from these simulations, it can be said that fluid properties such as brine composition, diffusion of various components in

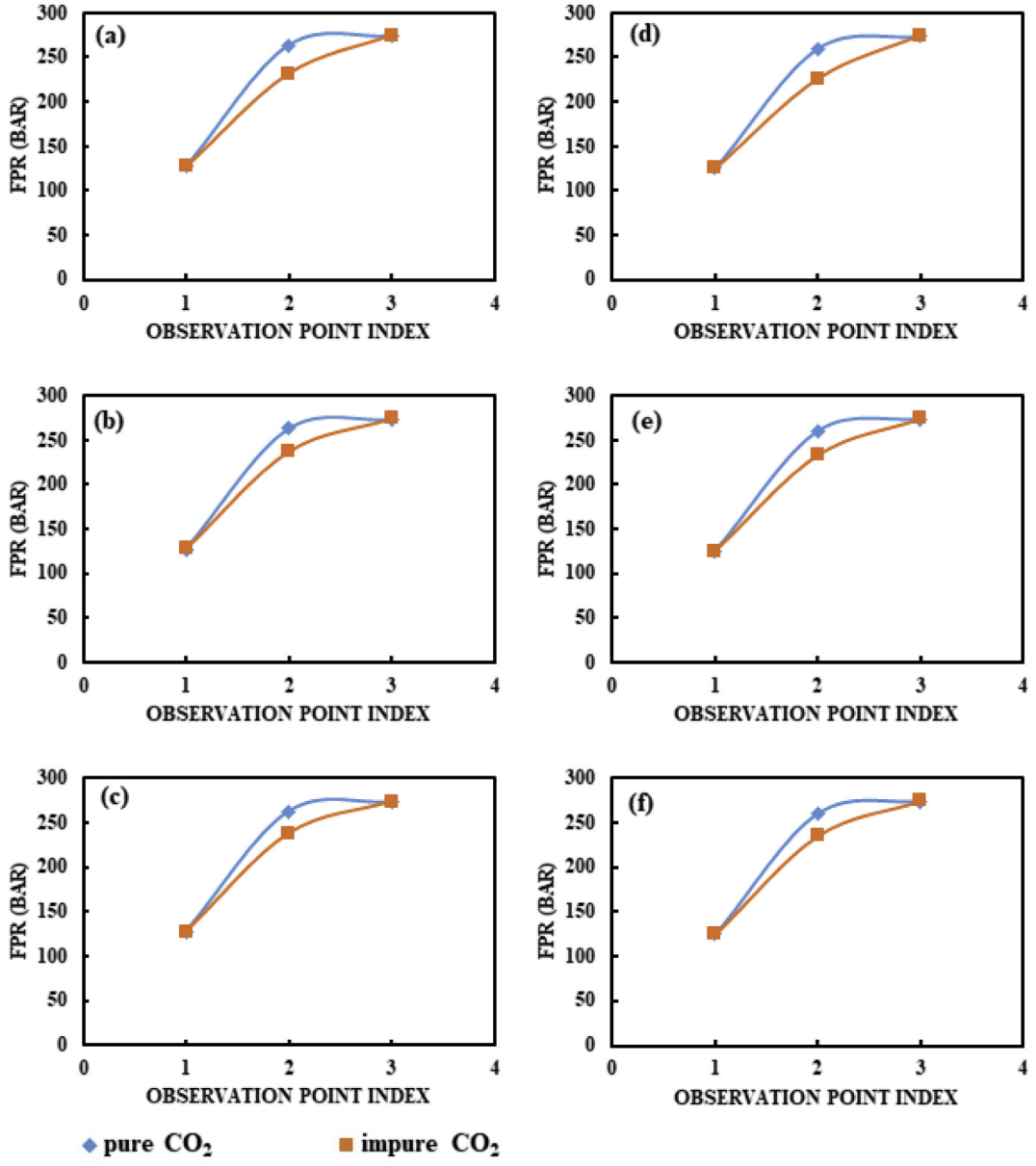

Figure 8. Field pressure (FPR) for pure and impure CO_2 storage for sites with 10% initial porosity ((a) CO_2–NO_2, (b) CO_2–SO_2, (c) CO_2–H_2S), and 22% initial porosity ((d) CO_2–NO_2, (e) CO_2–SO_2, (f) CO_2–H_2S).

both water and air, changes in viscosity, and interfacial tension, could all affect the reservoir performance to a certain degree. Though, the main cause of differences in the pressures and volumes (besides the properties of the storage formation) between pure and impure CO_2 injection is controlled by the volume of impurity within the CO_2 stream. Additionally, we observed that for all impurity cases simulated, the difference between target and actual injection rates is minimal and this can be due to the spatial variance in reservoir properties such as porosity and permeability and the implicit use of constant values for these properties in the model. Thus, the influence of non-linearity and heterogeneity as obtained in realistic settings is not considered in the model. This minimal difference between target and actual injection rates for the simplified models has been observed in a previous study on the BSF [25]. It is important to note that for all injection cases simulated, we monitored the cumulative CO_2 injected both at the end of injection and at the end of monitoring periods, without any noticeable discrepancy. Nonetheless, the use of simplified models will remain helpful in the evaluation of opportunities for CO_2 storage deployment in the UK offshore reservoir systems as a viable step toward decarbonisation of the global economy [25]. Due to its large areal extent, the BSF conforms with the use of simplified models to predict both regional and local reservoir behaviour in response to different injection scenarios.

4. Conclusions

The presence of impurities in the CO_2 stream can significantly affect the physical quality of the storage reservoir and it may also alter the molar volumes and shift the operational boundaries in the CO_2 phase diagram, affecting the limits of stability during injection operations. The main aim of this study was to evaluate the effect of CO_2 and impurities on reservoir performance during injection and storage in a sandstone saline aquifer. These included the evaluation of key performance indicators such as bottom-hole pressure, well gas injection rate, field pressure and cumulative injection for each impurity case. The results suggested that the effects of impurities influenced the reservoir performance but mostly at the early injection stages, but not the targeted injection rate. It was also

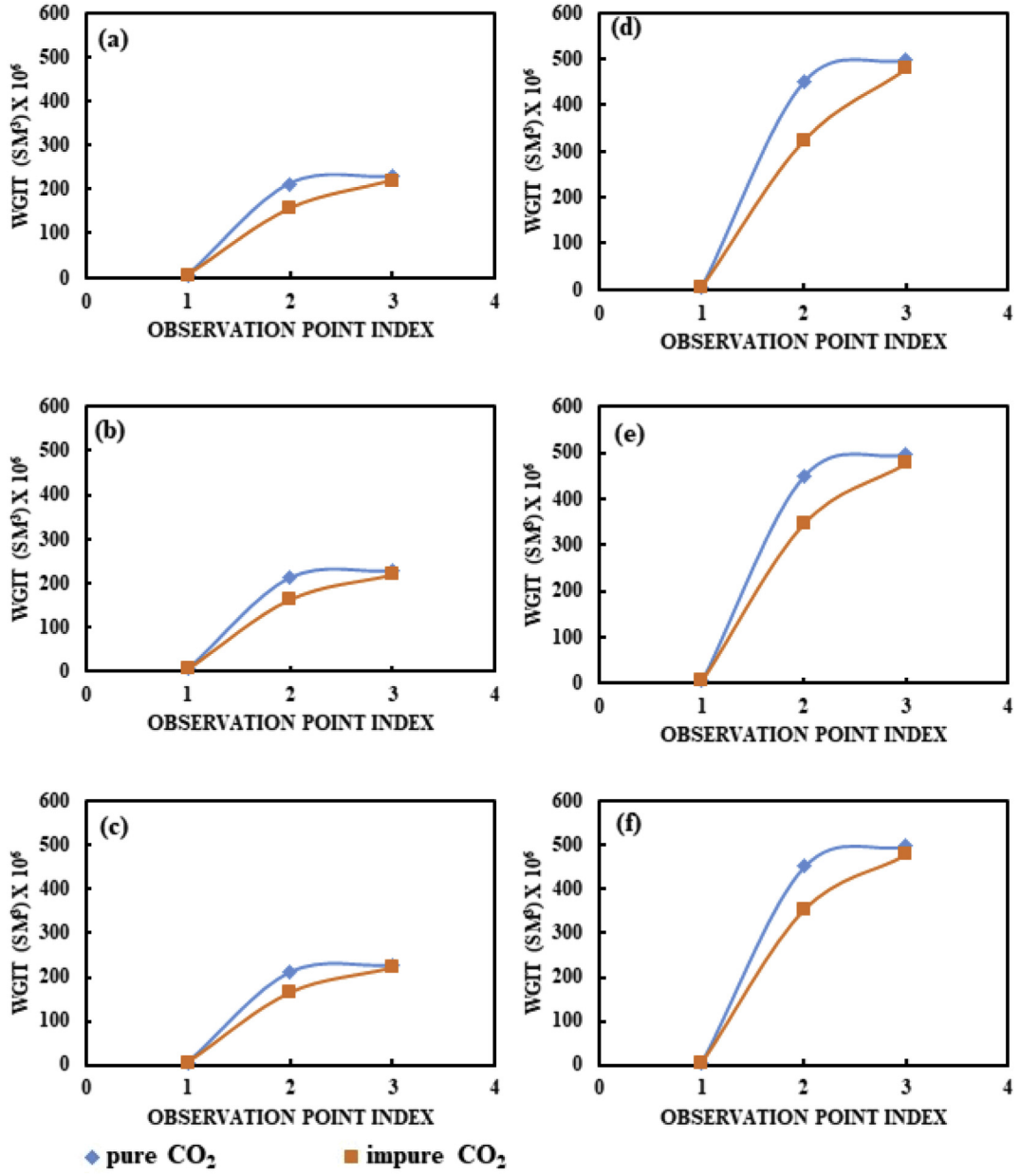

Figure 9. Well gas injection total (WGIT) for pure and impure CO_2 storage for sites with 10% initial porosity ((a) CO_2–NO_2, (b) CO_2–SO_2, (c) CO_2–H_2S), and 22% initial porosity ((d) CO_2–NO_2, (e) CO_2–SO_2, (f) CO_2–H_2S).

found that the porosity of the BSF significantly affected CO_2 injection. Additionally, it was observed that the effect of impurities does not affect the security of stored CO_2 as neither the injected volume nor field pressure were found to decrease 30 years after injection had ceased. We expect that the conclusions from this study can be extended to other saline aquifers with similar depositional- and post-depositional history.

Declarations

Author contribution statement

Mohammed Dahiru Aminu: Conceived and designed the experiments; Performed the experiments; Analyzed and interpreted the data; Wrote the paper.

Vasilije Manovic: Analyzed and interpreted the data.

Funding statement

Mohammed Dahiru Aminu is grateful to the Federal Government of Nigeria for sponsoring this research through the Petroleum Technology Development Fund (PTDF/E/OSS/PHD/AMD/724/14).

Competing interest statement

The authors declare no conflict of interest.

Additional information

No additional information is available for this paper.

Acknowledgements

The authors gratefully acknowledge the support of Schlumberger Information Solutions (UK) for donating ECLIPSE E300 Compositional Simulator which was used for conducting numerical modelling. We thank Dr Jan Vinogradov of the University of Aberdeen, Dr Ewan McAdam and Dr Seyed Ali Nabavi of Cranfield University for their constructive criticisms which helped to improve the quality of this work.

References

[1] IPCC, Special Report on Carbon Dioxide Capture and Storage, 2005. Cambridge.
[2] DECC, CCS Roadmap - Supporting Deployment of Carbon Capture and Storage in the UK, 2012.
[3] M.D. Aminu, S.A. Nabavi, C.A. Rochelle, V. Manovic, A review of developments in carbon dioxide storage, Appl. Energy 208C (2017) 1389–1419.
[4] S. Bachu, Sequestration of CO_2 in geological media: criteria and approach for site selection in response to climate change, Energy Convers. Manag. 41 (2000) 953–970.
[5] IEAGHG, Impact of Impurities on CO_2 Capture, Transport and Storage, 2004.
[6] G. Last, M. Schmick, Identification and Selection of Major Carbon Dioxide Stream Compositions, 2011.
[7] S. Waldmann, C. Hofstee, M. Koenen, D. Loeve, A. Liebscher, F. Neele, Physicochemical effects of discrete CO_2-SO_2 mixtures on injection and storage in a sandstone aquifer, Int. J. Greenh. Gas Control 54 (2016) 640–651.
[8] J. Wang, Z. Wang, D. Ryan, C. Lan, A study of the effect of impurities on CO_2 storage capacity in geological formations, Int. J. Greenh. Gas Control 42 (2015) 132–137.
[9] Z. Wang, J. Wang, C. Lan, I. He, V. Ko, D. Ryan, A. Wigston, A study on the impact of SO_2 on CO_2 injectivity for CO_2 storage in a Canadian saline aquifer, Appl. Energy 184 (2016) 329–336.
[10] J. Wang, D. Ryan, E.J. Anthony, N. Wildgust, T. Aiken, Effects of impurities on CO_2 transport, injection and storage, Energy Procedia 4 (2011) 3071–3078.
[11] S. Bachu, W.D. Gunter, E.H. Perkins, Aquifer disposal of CO_2: hydrodynamic and mineral trapping, Energy Convers. Manag. 35 (1994) 269–279.
[12] M. Bui, C.S. Adjiman, A. Bardow, E.J. Anthony, A. Boston, S. Brown, P.S. Fennell, S. Fuss, A. Galindo, L.A. Hackett, others, Carbon capture and storage (CCS): the way forward, Energy Environ. Sci. 11 (2018) 1062–1176.
[13] M.D. Aminu, S.A. Nabavi, V. Manovic, CO_2-brine-rock interactions: the effect of impurities on grain size distribution and reservoir permeability, Int. J. Greenh. Gas Control 78C (2018) 168–176.
[14] M. Jin, G. Pickup, E. Mackay, A. Todd, M. Sohrabi, A. Monaghan, M. Naylor, Static and dynamic estimates of CO_2-storage capacity in two saline formations in the UK, SPE J. 17 (2012) 1108–1118.
[15] J.M. Nordbotten, B. Flemisch, S.E. Gasda, H.M. Nilsen, Y. Fan, G.E. Pickup, B. Wiese, M.A. Celia, H.K. Dahle, G.T. Eigestad, K. Pruess, Uncertainties in practical simulation of CO_2 storage, Int. J. Greenh. Gas Control 9 (2012) 234–242.
[16] S.M. Shariatipour, Modelling of CO_2 Behaviour at the Interface between the Storage Formation and the Caprock, PhD Thesis, Heriot-Watt University, 2014.
[17] J.D.O. Williams, M. Jin, M. Bentham, G.E. Pickup, S.D. Hannis, E.J. Mackay, Modelling carbon dioxide storage within closed structures in the UK Bunter Sandstone Formation, Int. J. Greenh. Gas Control 18 (2013) 38–50.
[18] J.D.O. Williams, M. Bentham, M. Jin, G. Pickup, E. Mackay, D. Gammer, A. Green, The effect of geological structure and heterogeneity on CO_2 storage in simple 4-way dip structures; a modeling study from the UK southern North Sea, Energy Procedia 37 (2013) 3980–3988.
[19] C. Kolster, S. Agada, N. Mac Dowell, S. Krevor, The impact of time-varying CO_2 injection rate on large scale storage in the UK Bunter Sandstone, Int. J. Greenh. Gas Control 68 (2018) 77–85.
[20] J.T. Birkholzer, Q. Zhou, Basin-scale hydrogeologic impacts of CO_2 storage: capacity and regulatory implications, Int. J. Greenh. Gas Control 3 (2009) 745–756.
[21] H.E. Leetaru, S.M. Frailey, J. Damico, E. Mehnert, J. Birkholzer, Q. Zhou, P.D. Jordan, Understanding CO_2 plume behavior and basin-scale pressure changes during sequestration projects through the use of reservoir fluid modeling, in: Energy Procedia, 2009, pp. 1799–1806.
[22] ETI, Bunter Storage Development Plan, 2016.
[23] D.J. Noy, S. Holloway, R.A. Chadwick, J.D.O. Williams, S.A. Hannis, R.W. Lahann, Modelling large-scale carbon dioxide injection into the bunter sandstone in the UK southern North Sea, Int. J. Greenh. Gas Control 9 (2012) 220–233.
[24] D.J. Smith, D.J. Noy, S. Holloway, R.A. Chadwick, The impact of boundary conditions on CO_2 storage capacity estimation in Aquifers, in: Energy Procedia, 2011, pp. 4828–4834.
[25] S. Agada, S. Jackson, C. Kolster, N. Mac Dowell, G. Williams, H. Vosper, J. Williams, S. Krevor, The impact of energy systems demands on pressure limited CO_2 storage in the Bunter Sandstone of the UK Southern North Sea, Int. J. Greenh. Gas Control 65 (2017) 128–136.
[26] C.J. Vincent, Porosity of the Bunter Sandstone in the Southern North Sea Basin Based on Selected Borehole Neutron Logs, 2005.
[27] R. Mills, Self-diffusion in normal and heavy water in the range 1-45.deg, J. Phys. Chem. 77 (1973) 685–688.
[28] M. Holz, S.R. Heil, A. Sacco, Temperature-dependent self-diffusion coefficients of water and six selected molecular liquids for calibration in accurate 1H NMR PFG measurements, Phys. Chem. Chem. Phys. 2 (2000) 4740–4742.
[29] E. Guggenheim, The diffusion coefficient of sodium chloride, Trans. Faraday Soc. 50 (1954).
[30] W.A. Dekker, E. Snoeck, H. Kramers, The rate of absorption of NO_2 in water, Chem. Eng. Sci. 11 (1959) 61–71.
[31] A. Koliadima, J. Kapolos, L. Farmakis, Diffusion coefficients of SO_2 in water and partition coefficients of SO_2 in water–air interface at different temperature and pH values, Instrum. Sci. Technol. 37 (2009) 274–283.
[32] N. Haimour, O.C. Sandall, Molecular diffusivity of hydrogen sulfide in water, J. Chem. Eng. Data 29 (1984) 20–22.
[33] E.L. Cussler, Diffusion: Mass Transfer in Fluid Systems, second ed., Cambridge University Press, New York, 1997.
[34] Q. Zhou, J. Birkholzer, J. Rutqvist, C. Tsang, Sensitivity study of CO_2 storage capacity in brine aquifers with closed boundaries: dependence on hydrogeologic properties, in: Sixth Annu. Conf. Carbon Capture Sequestration, DOE/NETL, May, 2007, pp. 7–10.
[35] S. Holloway, C.J. Vincent, M.S. Bentham, K.L. Kirk, Top-down and bottom-up estimates of CO_2 storage capacity in the United Kingdom sector of the southern North Sea basin, Environ. Geosci. 13 (2006) 71–84.
[36] R.A. Chadwick, D.J. Noy, S. Holloway, Flow processes and pressure evolution in aquifers during the injection of supercritical CO_2 as a greenhouse gas mitigation measure, Petrol. Geosci. 15 (2009) 59–73.
[37] M.S. Bentham, A. Green, D. Gammer, The occurrence of faults in the bunter sandstone formation of the UK sector of the southern North Sea and the potential impact on storage capacity, in: Energy Procedia, 2013, pp. 5101–5109.
[38] J.D.O. Williams, S. Holloway, G.A. Williams, Pressure constraints on the CO_2 storage capacity of the saline water-bearing parts of the bunter Sandstone formation in the UK southern North Sea, Petrol. Geosci. 20 (2014) 155–167.
[39] N. Heinemann, M. Wilkinson, G.E. Pickup, R.S. Haszeldine, N.A. Cutler, CO_2 storage in the offshore UK bunter Sandstone formation, Int. J. Greenh. Gas Control 6 (2012) 210–219.
[40] P.M. Jarrell, C.E. Fox, M.H. Stein, S.L. Webb, Practical Aspects of CO_2 Flooding, Society of Petroleum Engineers Richardson, TX, 2002.
[41] M. Matuszewski, M. Woods, Quality Guidelines for Energy System Studies - CO_2 Impurity Design Parameters, 2012.
[42] E. de Visser, C. Hendriks, M. Barrio, M.J. Mølnvik, G. de Koeijer, S. Liljemark, Y. Le Gallo, Dynamis CO_2 quality recommendations, Int. J. Greenh. Gas Control. 2 (2008) 478–484.
[43] R.T.J. Porter, M. Fairweather, M. Pourkashanian, R.M. Woolley, The range and level of impurities in CO_2 streams from different carbon capture sources, Int. J. Greenh. Gas Control 36 (2015) 161–174.
[44] X. Jiang, A review of physical modelling and numerical simulation of long-term geological storage of CO_2, Appl. Energy 88 (2011) 3557–3566.
[45] R.C. Reid, J.M. Prausnitz, B.E. Poling, The Properties of Gases and Liquids, McGraw Hill Book Co., New York, NY, 1987.
[46] D.-Y. Peng, D.B. Robinson, A new two-constant equation of state, Ind. Eng. Chem. Fundam. 15 (1976) 59–64.
[47] Ö. Gündoğan, Geochemical Modelling of CO_2 Storage, Heriot-Watt University, 2011.
[48] A. Mathieson, J. Midgely, I. Wright, N. Saoula, P. Ringrose, In Salah CO_2 Storage JIP: CO_2 sequestration monitoring and verification technologies applied at Krechba, Algeria, Energy Procedia 4 (2011) 3596–3603.
[49] A. Mathieson, I. Wright, D. Roberts, P. Ringrose, Satellite imaging to monitor CO_2 movement at Krechba, Algeria, Energy Procedia 1 (2009) 2201–2209.
[50] J. Rutqvist, D.W. Vasco, L. Myer, Coupled reservoir-geomechanical analysis of CO_2 injection at in Salah, Algeria, Energy Procedia 1 (2009) 1847–1854.
[51] J. Carneiro, R. Martinez, I. Suaréz, Y. Zarhloule, A. Rimi, Injection rates and cost estimates for CO_2 storage in the west Mediterranean region, Environ. Earth Sci. 73 (2015) 2951–2962.
[52] A. Hosa, M. Esentia, J. Stewart, S. Haszeldine, Injection of CO_2 into saline formations: benchmarking worldwide projects, Chem. Eng. Res. Des. 89 (2011) 1855–1864.
[53] P. Stalder, Influence of crystallographic habit and aggregate structure of authigenic clay minerals on sandstone permeability, Geol. En Mijnb. 52 (1973) 217–220.
[54] W.L. Huang, A.M. Bishop, R.W. Brown, The effect of fluid/rock ratio on feldspar dissolution and illite formation under reservoir conditions, Clay Miner. 21 (1986) 585–601.
[55] L. Zhang, Y. Soong, R.M. Dilmore, Investigation on porosity and permeability change of Mount Simon sandstone (Knox County, IN, USA) under geological CO_2 sequestration conditions: a numerical simulation approach, Greenh. Gases Sci. Technol. 6 (2016) 574–587.
[56] M.T. Heald, R.E. Larese, The significance of the solution of feldspar in porosity development, J. Sediment. Petrol. 43 (1973) 458–460.
[57] P. Ringrose, Geological storage of CO_2: processes, capacity and constraints, in: How to Store CO_2 Undergr. Insights from Early-Mover CCS Proj, Springer, 2020, pp. 13–83.
[58] K. Shogenov, A. Shogenova, O. Vizika-Kavvadias, J.-F. Nauroy, Experimental modeling of CO_2-fluid-rock interaction: the evolution of the composition and properties of host rocks in the Baltic Region, Earth Sp. Sci. 2 (2015) 262–284.
[59] T.D. Rathnaweera, P.G. Ranjith, M.S.A. Perera, Experimental investigation of geochemical and mineralogical effects of CO_2 sequestration on flow characteristics of reservoir rock in deep saline aquifers, Sci. Rep. 6 (2016).
[60] L.N. Plummer, T.M.L. Wigley, D.L. Parkhurst, Kinetics of calcite dissolution in CO_2-water systems at 5 degree to 60 degree C and 0.0 to 1.0 atm. CO_2, Am. J. Sci. 278 (1978) 179–216.

[61] B. Lamy-Chappuis, B. Yardley, C. Grattoni, The effect of CO_2-fluid-rock interactions on the porosity and permeability of calcite-bearing sandstone, Am. Geophys. Union Fall Meet. 2013 (2013).
[62] G. Yang, Y. Li, A. Atrens, Y. Yu, Y. Wang, Numerical investigation into the impact of CO_2-water-rock interactions on CO_2 injectivity at the shenhua CCS demonstration project, China, Geofluids. 201 (2017) 17.
[63] S. Sadhukhan, P. Gouze, T. Dutta, Porosity and permeability changes in sedimentary rocks induced by injection of reactive fluid: a simulation model, J. Hydrol. 450–451 (2012) 134–139.
[64] J.P. Nogues, J.P. Fitts, M.A. Celia, C.A. Peters, Permeability evolution due to dissolution and precipitation of carbonates using reactive transport modeling in pore networks, Water Resour. Res. 49 (2013) 6006–6021.